CO adsorption-induced surface segregation and formation of Pd chains on AuPd(100) alloy: density functional theory based ising model and Monte Carlo simulations

Beien Zhu, Jérôme Creuze, Christine Mottet, Bernard Legrand, Hazar Guesmi

THE JOURNAL OF PHYSICAL CHEMISTRY C

Article

pubs.acs.org/JPCC

CO Adsorption-Induced Surface Segregation and Formation of Pd Chains on AuPd(100) Alloy: Density Functional Theory Based Ising Model and Monte Carlo Simulations

Beien Zhu,[*,†] Jerome Creuze,[‡] Christine Mottet,[§] Bernard Legrand,[∥] and Hazar Guesmi[*,⊥]

[†]Division of Interfacial Water and Key Laboratory of Interfacial Physics and Technology, Shanghai Institute of Applied Physics, Chinese Academy of Sciences, Shanghai 201800, China

[‡]ICMMO/SP2M, UMR8182, Univ Paris Sud, CNRS, Université Paris-Saclay, Bâtiments 410/420/430, rue du doyen Georges Poitou, 91405 Orsay cedex, France

[§]Aix-Marseille Université, CNRS, CINaM UMR 7325, Campus de Luminy, 13288 Marseille, France

[∥]CEA, DEN, Service de Recherches de Métallurgie Physique, Université Paris-Saclay, F-91191 Gif-sur-Yvette, France

[⊥]Institut Charles Gerhardt Montpellier, UMR 5253 CNRS/ENSCM/UM2/UM1, Matériaux Avancés pour la Catalyse et la Santé, 8 Rue de l'École Normale, 34296 Montpellier Cedex 5, France

ABSTRACT: In order to study how adsorption of CO molecules changes the surface composition of AuPd alloys, we develop a theoretical methodology which is able to take this effect into account. An Ising model based on density functional theory calculations is derived to define interatomic potentials that describe metal−metal, metal−CO, and CO−CO interactions. Then, through the use of Monte Carlo simulations within the semi-grand canonical ensemble, the effect of adsorption-induced segregation for the AuPd(100) surface is well-reproduced for different temperatures and CO pressures. Segregation isotherms identify a Pd surface enrichment for low CO pressures, and CO surface saturation is reached at an intermediate coverage of θ = 0.5 ML. Furthermore, Pd chains induced by an ordering of adsorbed CO molecules appear at low temperature and intermediate CO pressures. These chains are the result of a competitive effect between CO−CO repulsions and metal−CO interactions.

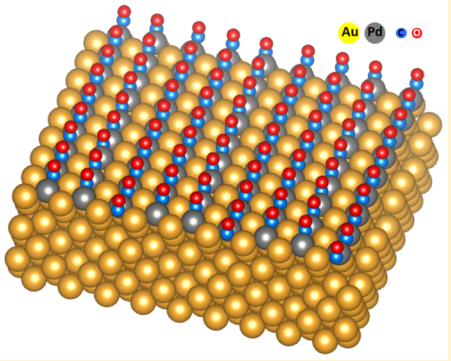

1. INTRODUCTION

Supported alloy nanoparticles are widely used as heterogeneous catalysts[1−3] by adding a second metal to a first one to improve its activity and/or selectivity. The optimization of these catalysts is determined by the control of the distribution of the constituents on the surface during the preparation and under the reaction conditions. Thus, the surface segregation phenomenon, i.e., the enrichment of the surface with one of the elements of the alloy, is of considerable importance. Also important is the understanding of segregation phenomena induced by the presence of gas molecules adsorbed on the surface.[4−6] Indeed, the reactive environment where catalysis occurs can further modify the chemical composition of the surface if one alloy component interacts more strongly with a gas-phase species than the others. This so-called adsorbate-induced segregation phenomenon is crucial to understand and correctly predict the properties and functions of alloy catalysts under working conditions. Surprisingly, while surface segregation in nanoalloys is the subject of several theoretical works in vacuum conditions,[7−9] this is not yet the case under reaction conditions.[10]

Among bimetallic systems, gold alloyed with palladium has received particular attention because of its use in many catalytic reactions. For instance, in the selective reduction reaction of NO_x species, the addition of Pd to Au may provide N−O bond-breaking capability,[11] which is not the case over monometallic gold catalyst.[12] Similarly, for the case of low-temperature CO oxidation reaction, because Pd is known to dissociate O_2 at temperature as low as 150 K,[13] the idea of adding Pd to Au to favor the dissociation of O_2 is prone to improve the catalytic properties of gold. However, to optimize the beneficial synergetic effect of the addition of Pd it is crucial to predict and to control its amount and its distribution on the gold particle surface.

From the thermodynamics point of view, while gold tends to segregate at the surface of AuPd alloys under vacuum conditions,[9,14,15] a reverse segregation of Pd occurs upon exposure to reactive gases. For instance, Goodman's group has reported that a significant proportion of Pd segregates on AuPd(100) alloy surface after exposition to gas-phase CO pressure of 0.1 Torr.[16,17] The authors suggest that segregated Pd atoms are the active sites that catalyze CO oxidation reaction. They argue that contiguous Pd atoms bind and dissociate the O_2 molecules, supplying O atoms for CO

Received: October 16, 2015
Revised: December 10, 2015
Published: December 11, 2015

DOI: 10.1021/acs.jpcc.5b10158
J. Phys. Chem. C 2016, 120, 350−359

adsorbed on Au sites and improving CO oxidation at room temperature. In a recent work,[18] we have investigated the surface configuration of Pd atoms in AuPd nanoparticles during CO gas exposure. Using a combined diffuse reflectance Fourier transform spectroscopy and density functional theory (DFT) approach, we have evidenced a Pd surface enrichment due to the strong adsorption of CO and we have demonstrated that only isolated Pd and Pd dimers may exist in the surface of AuPd nanoparticles for low Pd content. In addition, other previous works of the group were devoted to the understanding of the energetic and the electronic structure of reversed Pd segregations in the presence of several reactive gases such as CO, O, and O_2.[19−21]

In order to provide a landscape of the surface in equilibrium with the gas phase and to go further in the understanding of this intriguing phenomenon, it is important to correctly describe the metal segregation first under vacuum and at 0 K and then at a given temperature and gas pressure. In a recent paper,[22] we have developed DFT calculations to evaluate the energetic key quantities of the AuPd system under vacuum condition, i.e., segregation enthalpies for the (100) and (111) surfaces and effective pair interactions in the bulk and in the surfaces. We have analyzed the segregation driving forces in the two infinite dilute limits of the Au−Pd alloy for both (100) and (111) surfaces. We have shown that the decomposition of the segregation enthalpy into its different elementary contributions, which is generally investigated by semiempirical methods,[23,24] is still valid at the ab initio level of description.

We devote the present work to the study of the effect of gas on the alloy surface. More precisely, we develop a theoretical method which is able to evaluate the surface composition of a bimetallic alloy as a function of both the bulk composition and the partial pressure of the gas. In this paper, we illustrate this approach by considering the AuPd system and Pd segregation occurring in the presence of CO. To study how adsorption of CO molecules changes the surface composition of AuPd alloys, we build a DFT-based Ising model with interatomic potentials able to describe both the interactions between the metal atoms in the alloy, those between the metal atoms in the surface and the adsorbed molecules and those between the adsorbed molecules. Thus, all databases concerning the segregation energies, mixing energies, and adsorption energies are calculated using accurate DFT optimizations. Furthermore, we use Monte Carlo simulations to obtain segregation isotherms and to get information on the evolution of the Pd surface concentration with the Pd bulk concentration as a function of the CO coverage.

The present paper is organized as follows: in section 2, we present the technical details of the DFT calculations and the Ising model used to perform the Monte Carlo simulations. In section 3, detailed DFT calculations on the AuPd(100) surface are reported. All energetic terms for the metal−metal, metal−CO, and CO−CO interactions that define the Ising Hamiltonian are explicitly identified. We also present the Monte Carlo simulations, first on the monometallic Au and Pd (100) surfaces exposed to CO gas and then on the AuPd(100) surface. One of the original results is the formation of regular Pd chains with CO bridging contiguous Pd atoms. The predicted configuration is analyzed in detail and discussed in the light of the experimental observations.

2. THEORETICAL METHODS

2.1. First-Principles Calculations. Extensive periodic DFT calculations are performed using the Vienna ab initio simulation package (VASP).[25] The exchange−correlation energy is calculated within the local density approximation as parametrized by Perdew and Zunger (LDA-PZ).[26] The choice of LDA is justified in the next section. The valence electrons are treated explicitly, and their interactions with the ionic cores are described by the projector augmented-wave method (PAW),[27,28] allowing the use of a low energy cut off equal to 415 eV for the plane-wave basis. The positions of the atoms in the super cell are relaxed until the total energy differences fall below 10^{-4} eV.

To model the pure metallic Au(100) surface and the AuPd(100) bimetallic one, a slab of 108 atoms is used, containing six atomic layers representing a 3 × 3 supercell, separated by 15 Å of vacuum space. Atomic relaxation of all metallic atoms in the top four layers of the slab and the CO molecules is allowed. The bottom two layers are constrained at the bulk geometry. Other details on the computed model can be found in our previous works.[18,19]

2.2. Ising Model for the Interaction Potential. To describe the energy part of an A_cB_{1-c}-gas system (here A = Pd, B = Au, and gas = CO), we use an Ising Hamiltonian in which only effective nearest-neighbor pair interactions are taken into account:

$$H = \frac{1}{2}\sum_{n,m\neq n}^{i,j} P_n^i P_m^j V^{ij} \tag{2.1}$$

where V^{ij} is the interaction energy between a species of type i at site n and a species of type j at site m; i and j represent A atom, B atom, or gas molecule; and n and m are in the nearest-neighbor position. p_n^i is the occupation number that equals 1 (0) if the site n is (not) occupied by a specie of type i. Considering that for a binary alloy $p_n^A = 1 - p_n^B = p_n$ and by setting $p_n^{gas} = q_n$, the Hamiltonian H can be written as the sum of three contributions:

$$H = H_{alloy} + H_{alloy-gas} + H_{gas} \tag{2.2}$$

where

$$H_{alloy} = H_0 + (\tau - V)\sum_n p_n + V\sum_{n,m\neq n} p_n p_m \tag{2.3}$$

$$H_{alloy-gas} = \frac{1}{2}(V^{Bgas}\sum_{n'} q_{n'} + \tau'\sum_{n,n'} p_n q_{n'}) \tag{2.4}$$

$$H_{gas} = \frac{1}{2}V^{gasgas}\sum_{n',m'\neq n'} q_{n'}q_{m'} \tag{2.5}$$

$H_0 = (1/2)\sum_{n,m\neq n}V^{BB}$ and $\tau = (1/2)(V^{AA} - V^{BB})$ is proportional to the difference between cohesive energies of pure metals. $V = (1/2)(V^{AA} + V^{BB} - 2V^{AB})$ is the alloying pair interaction that characterizes the tendency of the alloy to favor homoatomic ($V < 0$) or heteroatomic ($V > 0$) pairs, and $\tau' = (V^{Agas} - V^{Bgas})$ is proportional to the difference between adsorption energies of the gas molecule on pure metals. In these expressions, the (un)primed indices stands for the adsorbate (metal) lattice.

As described in the Introduction, all the energetic quantities are obtained by means of DFT calculations. Thus, the main

DOI: 10.1021/acs.jpcc.5b10158
J. Phys. Chem. C 2016, 120, 350−359

features of the AuPd system are reproduced by taking $\tau = (1/2)(V^{AuAu} - V^{PdPd}) = 0.0617$ eV and $V = 0.029$ eV.[22]

At this point, we can note that the pair interaction energies V^{ij} are defined as independent from the local environment surrounding the species involved in the pair, as usual in such an approach. As we will see later, if this turns out to be reasonable for the metal−metal and metal−CO interactions, this is not the case for the CO−CO interactions for which it is necessary to account for the underlying metallic environment.

2.3. Monte Carlo Simulation Procedure. To determine the distribution of Pd and Au atoms on the different sites of the simulation box, we perform Monte Carlo (MC) simulations where the nominal concentration of the Pd_cAu_{1-c} alloy is fixed by the chemical potential difference[29] $\Delta\mu_{AuPd} = \mu_{Pd} - \mu_{Au}$. The simulations are performed within the semi-grand canonical (s-GC) ensemble in which the total number of metallic species ($N = N_{Au} + N_{Pd}$), temperature (T), and pressure (P) are fixed. The partial number of each kind of atom (N_{Au}, N_{Pd}) is changed by varying $\Delta\mu_{AuPd}$. In order to take into account the effect of the CO gas, we consider adsorption and desorption of CO molecules on the alloy surface. For this purpose, we introduce the chemical potential difference for the gas, $\Delta\mu_{CO}$. The CO chemical potential is related to the temperature and the pressure by assuming that the surface is in thermodynamic equilibrium with the gas phase. Considering CO as an ideal gas reservoir, the temperature and pressure dependence of $\Delta\mu_{CO}(T, P_{CO})$ can be determined by

$$\Delta\mu_{CO}(T, P_{CO}) = H(T, P^0) - H(0\text{K}, P^0) - TS(T, P^0) + RT\ln(P_{CO}/P^0) \quad (2.6)$$

where the enthalpy H and the entropy S of CO are calculated from the tabulated values of the JANAF thermodynamics tables,[30] P^0 being the pressure of the reference state (1 bar).

The simulated system is a slab of 15 layers consisting of 10 × 10 × 13 atoms in a fcc (100) crystal structure with a fixed lattice parameter of 4.07 Å and two adsorbate layers on the top/bottom of the slab for the CO adsorption. A standard Metropolis algorithm is used,[31] and the averages are evaluated over 100 MC macrosteps, a similar number of macrosteps being used to reach equilibrium. A MC macrostep involves $1000 \times N_s$ to $5000 \times N_s$ propositions of chemical switches, N_s being the total number of sites in the slab.

As will be discussed in the next section, we consider only one kind of adsorption site for the CO molecules in this work, which is the bridge site on the (100) surface. For each site in the adsorbate layers, there are two possible states: free or occupied by a CO molecule. For each site in the alloy, there are also two possibilities: occupied by a Pd or an Au atom. Thus, in our MC simulations we have two trials:

(i) The chemical identity of a site in the alloy is changed with relative probability

$$\frac{\Gamma_{new}}{\Gamma_{old}} = \exp\{-[\Delta U - (N_{Pd}^{new} - N_{Pd}^{old})\Delta\mu_{AuPd}]/kT\} \quad (2.7)$$

where N_{Pd}^{new} and N_{Pd}^{old} are the numbers of Pd atoms in the new and the old state, respectively.

(ii) One CO molecule is adsorbed/desorbed on/from a site in the adsorbate layers with relative probability

$$\frac{\Gamma_{new}}{\Gamma_{old}} = \exp\{-[\Delta U - (N_{CO}^{new} - N_{CO}^{old})\Delta\mu_{CO}]/kT\} \quad (2.8)$$

where N_{CO}^{new} and N_{CO}^{old} are the numbers of CO molecules in the new and the old state, respectively.

In eqs 2.7 and 2.8, ΔU is the energy balance between the new and old states and kT is the Boltzmann factor.

3. RESULTS AND DISCUSSION

3.1. DFT Calculations. Local density approximation (LDA) is considered in this work because of its better description of the surface energies of the alloy constituents (Au and Pd) as compared to generalized gradient approximation (GGA). As reported in Table 1, both methods underestimate the surface energies of Au, but LDA predicts an accurate surface energy for Pd(100). In addition, for Au, performance of GGA for the bulk binding energy is even worse, E_{coh}(GGA) = −3.05 eV versus experimental −3.81 eV;[32] concomitantly, E_{coh}(LDA) = −4.24 eV becomes somewhat closer to the experiment.

Table 1. Computed DFT and Experimental Values of the Lattice Parameters (a_0, Å), Cohesive Energies (E_{coh}, eV/atom), and Surface Energies (γ_{surf}, eV/atom) of Au and Pd[a]

	experiment	GGA-PBE	LDA-PZ
		Au	
a_0 (Å)	4.08[32]	4.17 (+2.2%)	4.07 (−0.2%)
E_{coh} (eV/atom)	−3.81[32]	−3.05 (−20%)	−4.24 (+11%)
$\gamma_{surf(100)}$ (eV/atom)	0.88[33]	0.46 (−48%)	0.65 (−26%)
		Pd	
a_0 (Å)	3.89[32]	3.96 (+1.8%)	3.85 (−1.0%)
E_{coh} (eV/atom)	−3.89[32]	−3.74 (−3.8%)	−4.98 (+28%)
$\gamma_{surf(100)}$ (eV/atom)	0.95[33]	0.73 (−23%)	0.95 (0%)

[a]The percentages indicated in the parentheses correspond to the shifts from the experimental values.

Considering the interaction of a single CO molecule with the metallic surface, we have analyzed within local density approximation all possible adsorption sites of the (100) surface. Over the monometallic Au(100) surface, DFT calculations predict the bridge site to be the most favorable adsorption site. As depicted in Table 2, the adsorption energies of CO on gold surface are −1.03 eV and −1.29 eV on top and on bridge sites, respectively. When considering the presence of one Pd atom in the Au(100) surface, the adsorption energies are higher (in absolute value) by 0.81 and 0.64 eV for the top and the bridge positions, respectively. Despite the strong affinity of CO for Pd,[19] it prefers to bridge one gold atom and one Pd atom instead of binding on top of the Pd atom. However, when one considers contiguous Pd atoms (a dimer of Pd), two equivalent sites (−2.57 eV) are found for CO adsorption, the bridging site between two Pd atoms and the top of one of the two Pd atoms. Finally, on a pure Pd surface, CO prefers the 4-fold site with an adsorption energy value of −2.84 eV. The adsorption energy on

Table 2. Computed DFT/LDA Adsorption Energies (E_{ads}, eV) of CO on Monometallic Au(100) and Pd(100) and in the Presence of One and Two Pd Atoms in the Au(100) Surface

E_{ads}-CO (eV)	top	bridge	4-fold
monometallic Au(100)	−1.03	−1.29	unstable
one Pd in the Au(100) surface	−1.84	−1.93	unstable
dimer Pd in the Au(100) surface	−2.57	−2.57	unstable
monometallic Pd(100)	−2.09	−2.72	−2.84

DOI: 10.1021/acs.jpcc.5b10158
J. Phys. Chem. C 2016, 120, 350−359

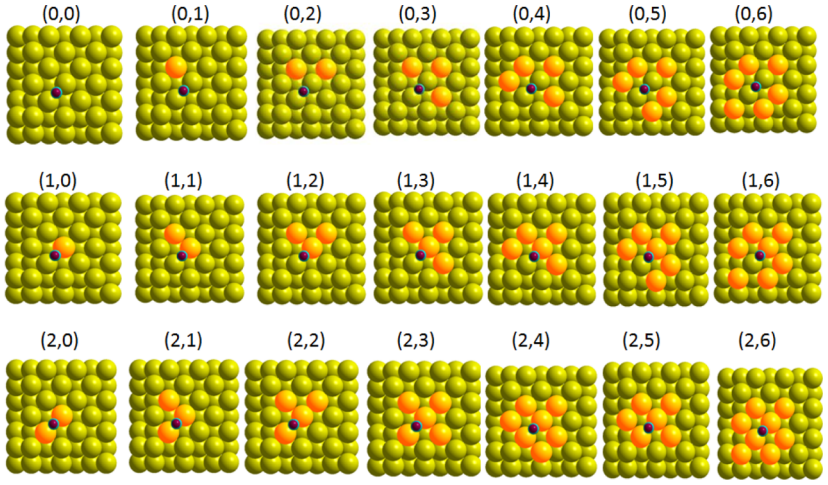

Figure 1. Snapshots of a CO molecule adsorbed on a bridge site of the AuPd(100) surface with different Pd surface concentrations (C-end adsorption). Gold, palladium, carbon, and oxygen atoms are represented by yellow, orange, blue, and red balls, respectively. Values in parentheses (m, n) represent the evolution of the number of surface Pd atoms in CO's nearest-neighbor position (m) and CO's next-nearest-neighbor position (n).

the bridge site is only 0.13 eV lower (in absolute value) than on the 4-fold site. For the sake of simplicity, only the bridge position will be considered in the present work.

3.1.1. CO Adsorption versus Surface Pd Concentration. To evaluate how adsorption of CO can be affected by the presence of Pd in the AuPd(100) surface (and vice versa), we calculate the evolution of the CO adsorption energy as a function of the Pd surface concentration. For this, we start by considering a CO molecule adsorbed on a bridge site of the monometallic Au(100) surface, and we increase one by one the number of Pd in CO's nearest-neighbor and next-nearest-neighbor positions, respectively. By doing this, we generate a (m, n) matrix of AuPd surfaces as shown in Figure 1, where m represents the number of surface Pd atoms in CO's nearest-neighbor position (Pd^{1st}) and n represents the number of surface Pd atoms in CO's next-nearest-neighbor position (Pd^{2nd}), the maximum for bridge site on the (100) surface being 2 and 6, respectively. Consequently, (0, 0) refers to CO adsorbed on a bridge site of the pure Au surface with no Pd in nearest nor next-nearest-neighbor position and (2, 6) refers to CO adsorbed on a bridge site with two Pd atoms in nearest-neighbor position and six Pd atoms in next-nearest-neighbor position.

The DFT adsorption energy values of all computed configurations (see Figure 1) are plotted in Figure 2 as a function of the number of Pd atoms in CO's nearest-neighbor position m (0, 1, 2) and next-nearest-neighbor position n (0, 1, 2,..., 6).

Figure 2 reveals several points worth mentioning. First, the evolution of the adsorption energies of CO as a function of the number of Pd atoms in nearest-neighbor position (m) follows three straight lines, showing a linear relationship between the adsorption energy and m. Given that the positions of the next-nearest-neighbors (n) are chosen randomly, the linear relationship indicates that the adsorption energy does not depend on the position of the next-nearest-neighboring of Pd atoms but depends on only their number. This scaling relation as a function of the local chemical environment is specific to alloy materials and should be different from the structure-sensitive scaling relation that was recently reported on monometallic systems.[34,35]

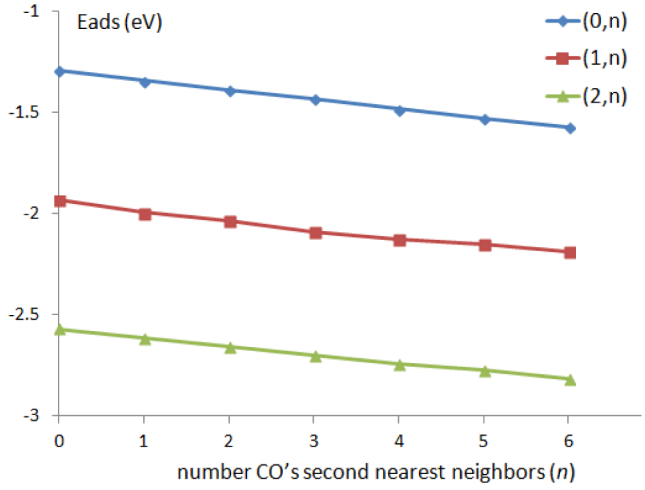

Figure 2. Evolution of the adsorption energies of CO on all computed configurations (cf. Figure 1) plotted as a function of the number of Pd atoms in CO's next-nearest-neighbor position n, ranging from 0 to 6, for each value of m: m = 0 (blue diamonds), m = 1 (red squares), and m = 2 (green triangles).

According to our DFT results, the equation defining the evolution of the CO interaction with the alloy as a function of the local Pd environment ($H_{alloy-gas}$ in our Ising model) can be written as follows:

$$E_{ads}(m, n) = E_{ads}^{Au} + mV_{CO-Pd}^{1st} + nV_{CO-Pd}^{2nd} \quad (3.1)$$

where V_{CO-Pd}^{1st} and V_{CO-Pd}^{2nd} are the energy contributions of additional Pd atoms in nearest- and next-nearest-neighbor positions, respectively. V_{CO-Pd}^{1st} corresponds to the gap between the three curves (for a fixed m), while V_{CO-Pd}^{2nd} is the mere slope of each line in Figure 2. Note that eq 3.1 is obtained by choosing the adsorption energy of CO on the pure Au(100) surface (E_{ads}^{Au}) as the reference. Thus, according to our results (E_{ads}^{Au} = −1.29 eV, V_{CO-Pd}^{1st} = −0.64 eV, and V_{CO-Pd}^{2nd} = −0.04 eV), eq 3.1 can be written as

$$E_{ads}(m, n) = -1.29 - 0.64m - 0.04n \quad (3.2)$$

DOI: 10.1021/acs.jpcc.5b10158
J. Phys. Chem. C 2016, 120, 350−359

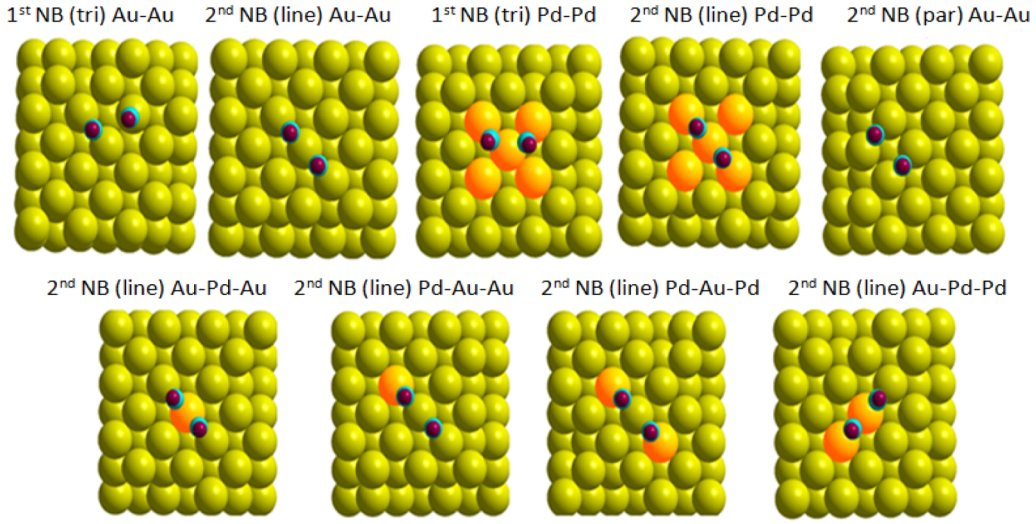

Figure 3. Relaxed configurations of two coadsorbed CO molecules on the (100) surface obtained by DFT calculations.

Table 3. DFT-Computed Adsorption Energies (E_{ads}) of the Configurations Reported in Figure 3[a]

	1st NB(tri) Au−Au	2nd NB(line) Au−Au	1st NB(tri) Pd−Pd	2nd NB(line) Pd−Pd	2nd NB(par) Au−Au
E_{ads} (eV)	−2.32	−2.45	−4.94	−5.12	−2.58
E_{ads}^{isol} (eV)	−2.58	−2.58	−5.40	−5.40	−2.58
ΔE_{ads} (eV)	0.26	0.13	0.46	0.28	0.00
	2nd NB(line) Au−Pd−Au	2nd NB(line) Pd−Au−Au	2nd NB(line) Pd−Au−Pd	2nd NB(line) Au−Pd−Pd	
E_{ads} (eV)	−3.63	−3.10	−3.79	−4.30	
E_{ads}^{isol} (eV)	−3.86	−3.22	−3.86	−4.50	
ΔE_{ads} (eV)	0.23	0.12	0.07	0.20	

[a] E_{ads}^{isol} is calculated by eq 3.1 and $\Delta E_{ads} = E_{ads} - E_{ads}^{isol}$.

The simple linear relationship between the adsorption energy and the number of Pd surface atoms allows us to treat the CO−metal interactions even more simply in the MC model. We can describe E_{ads} by two effective pair interactions between CO and its nearest-neighboring Au and Pd atoms. $V_{CO-Au}^{eff} = -0.65$ eV, given by half of E_{ads}^{Au} because it is a bridge site, and $V_{CO-Pd}^{eff} = -1.29$ eV, derived from $V_{CO-Au}^{eff} + V_{CO-Pd}^{1st}$. The effect of the next-nearest-neighboring of Pd atoms can be neglected because the value of the interaction is very small (0.04 eV).

3.1.2. Effect of CO−CO Repulsion. On the basis of the above results, the change in adsorption energy induced by the addition of a second adsorbed CO molecule is investigated. For the (100) surface, three possible cases of 2 coadsorbed CO molecules are considered (see Figure 3).

(i) In the first case, the two CO molecules are located on two bridge sites in nearest-neighbor position, forming a CO−metal−CO triangle chain (1st NB(tri)).

(ii) In the second case, the two CO molecules are located on two bridge sites in next-nearest-neighbor position and share one metal atom, forming a CO−metal−CO linear chain (2nd NB(line)).

(iii) The third case is similar to the second one, except that the two CO molecules share no metal atom (2nd NB(para)).

As shown in Figure 3, the three cases are also considered for different Pd surface distributions. The calculated adsorption energies of the configurations listed in Figure 3 are presented in Table 3. In addition, the adsorption energies of two isolated CO molecules are depicted:

$$E_{ads}^{isol} = \sum_{i=1}^{2} E_{ads}^{i}(m_i, n_i) \tag{3.3}$$

where $E_{ads}^{i}(m_i,n_i)$ is the adsorption energy of the i^{th} CO molecule, calculated by eq 3.1, and ΔE_{ads} is the difference between the direct DFT calculation and E_{ads}^{isol}. This energy difference is positive and represents the repulsion strength between the coadsorbed CO molecules as calculated by DFT.

As an example, E_{ads}^{isol} of configuration 1st NB(tri)Au−Au is calculated as the sum of two configurations with a single CO molecule bridging Au atoms (configuration (0, 0) of Figure 1) and E_{ads}^{isol} of configuration 2nd NB(line)Au−Pd−Pd is calculated as the sum of the configuration (1,0) and (2,0).

As reported in Table 3, ΔE_{ads} is equal to zero when the two CO molecules share no metal atom. This indicates that lateral adsorbate interactions should be taken into account only when the two CO molecules share a metal atom. Moreover, ΔE_{ads} for two CO molecules in nearest-neighbor position is stronger than ΔE_{ads} for two CO molecules in next-nearest-neighbor position. This can be easily understood by the fact that closer CO molecules have stronger repulsion. Finally, we find that ΔE_{ads} is related to the chemical type of the shared metal atom: it is stronger when two CO molecules share one Pd atom. This is expected because Pd pulls CO closer to the surface, due to the stronger Pd−CO interaction which leads to a reduction of the CO−CO distance.

The above analysis of ΔE_{ads} and therefore of the CO−CO repulsions allows us to fit an effective CO−CO interaction as in the following:

DOI: 10.1021/acs.jpcc.5b10158
J. Phys. Chem. C 2016, 120, 350−359

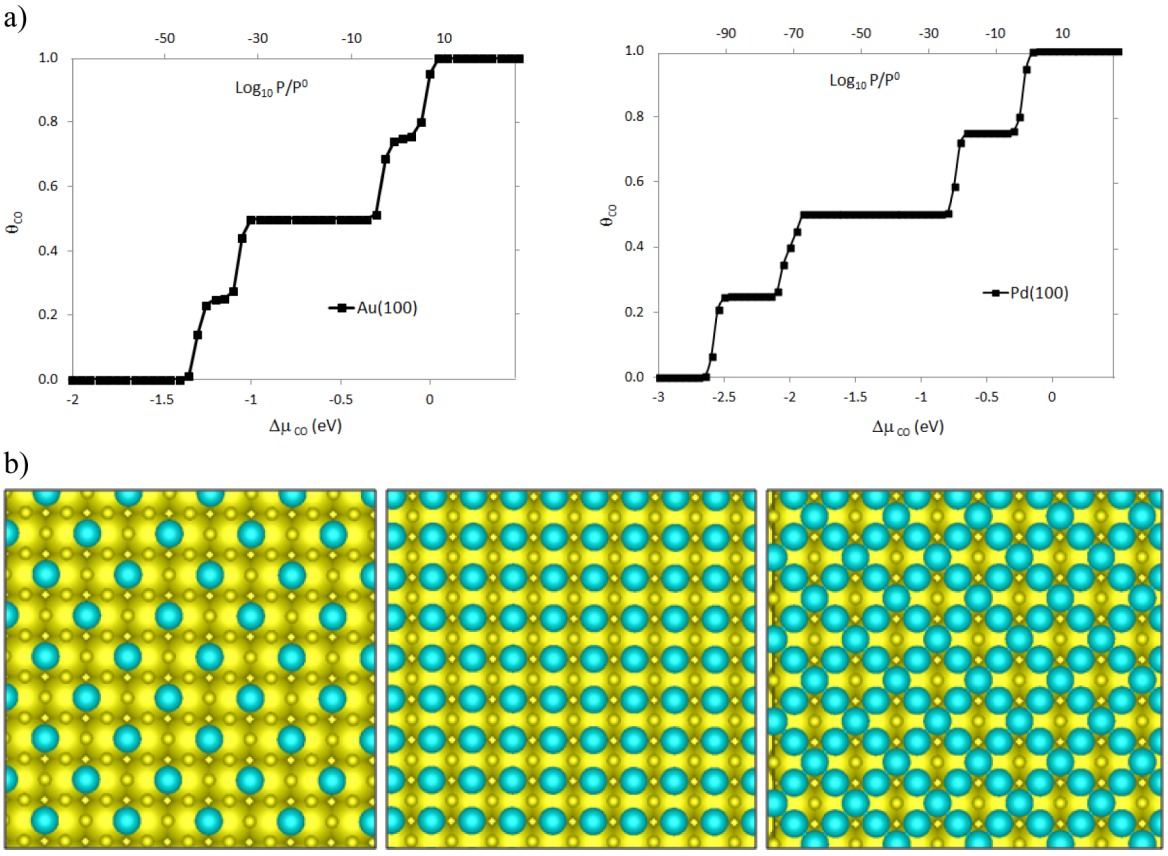

Figure 4. (a) Adsorption isotherms representing the CO coverage (θ_{CO}) as a function of the chemical potential ($\Delta\mu_{CO}$) on the pure Au(100) surface (upper left) and the pure Pd(100) surface (upper right) at T = 100 K. (b) The three ordered configurations related to the three plateaus in the isotherms at θ = 0.25, 0.5 and 0.75: metallic surface (big yellow balls), filled bridge adsorption sites (blue balls), and vacant bridge adsorption sites (small yellow balls), respectively.

$$\begin{cases} V^{\text{eff}}_{\text{CO-CO}}(\text{1NB, Au}) = 0.26 \text{ eV},\ V^{\text{eff}}_{\text{CO-CO}}(\text{1NB, Pd}) \\ \quad = 0.46 \text{ eV} \\ V^{\text{eff}}_{\text{CO-CO}}(\text{2NB, Au}) = 0.11 \text{ eV},\ V^{\text{eff}}_{\text{CO-CO}}(\text{2NB, Pd}) \\ \quad = 0.25 \text{ eV} \end{cases} \tag{3.4}$$

These $V^{\text{eff}}_{\text{CO-CO}}$ values depend on two parameters: the positions of the two CO molecules (nearest-neighbor or next-nearest-neighbor) and the chemical type of the shared metal atom. Each value is taken as the average value of the corresponding ΔE_{ads} in Table 3. If there is no shared metal atom, $V^{\text{eff}}_{\text{CO-CO}} = 0$ eV.

Finally, using the three effective pair interactions $V^{\text{eff}}_{\text{CO-Au}}$, $V^{\text{eff}}_{\text{CO-Pd}}$, and $V^{\text{eff}}_{\text{CO}(i)-\text{CO}(j)}$ discussed above, the adsorption energy of CO on a AuPd(100) surface with given CO coverage and Pd concentration can be written as

$$E_{\text{ads}} = \sum_i ((2 - m_i)V^{\text{eff}}_{\text{CO-Au}} + m_i V^{\text{eff}}_{\text{CO-Pd}}) + \frac{1}{2}\sum_{i,j\neq i} V^{\text{eff}}_{\text{CO}(i)-\text{CO}(j)} \tag{3.5}$$

The first term describes the interactions between the i^{th} CO molecule and its nearest-neighboring metal atoms. For the bridge site, one CO molecule interacts with two surface metal atoms; thus, m_i and $(2 - m_i)$ are the numbers of Pd and Au atoms interacting with the i^{th} CO molecule, respectively. The second term corresponds to the CO−CO interactions between the i^{th} and j^{th} CO molecules, $V^{\text{eff}}_{\text{CO}(i)-\text{CO}(j)}$. We note that the latter eq 3.5 is simply the sum of $H_{\text{alloy-gas}} + H_{\text{gas}}$ where the gas Hamiltonian term includes the effect of the underlying metallic environment.

This adsorption energy is exactly the energy balance given by the adsorption/desorption process of a CO molecule on the surface. It is determined by both the surface composition and the CO coverage. Considering all the above energetic terms, the CO adsorption-induced change or permutation of a gold surface atom into a palladium one can be written as the following energy difference:

$$\Delta H^{\text{perm,ads}} = N_{\text{CO}}(V^{\text{eff}}_{\text{CO-Pd}} - V^{\text{eff}}_{\text{CO-Au}}) + \sum_{i,j} \Delta V^{\text{eff}}_{\text{CO}(i)-\text{CO}(j)} \tag{3.6}$$

where N_{CO} is the number of CO molecules interacting with the permuted atom. Because the CO−CO interaction is found to be dependent on the chemical type of the shared surface metal atom, the permutation of a surface atom will also change its nearest-neighboring CO−CO interaction, which induces the second term in eq 3.6. This is the first time that the connection between the CO−CO repulsion and the surface composition is revealed. Therefore, we can expect a competition between CO−metal interaction and CO−CO repulsion because the stronger CO−Pd interaction results in an increase of $V^{\text{eff}}_{\text{CO-CO}}$. We will discuss this competition and its consequence in more detail with the Monte Carlo results in the next section.

3.2. Monte Carlo Results. *3.2.1. CO Adsorption on Monometallic (100) Surfaces.* To verify that CO adsorption is well-described by our Monte Carlo procedure, we first investigate the adsorption on the monometallic Au(100) and

DOI: 10.1021/acs.jpcc.5b10158
J. Phys. Chem. C 2016, 120, 350−359

Pd(100) surfaces. This allows us to evaluate the ordering of the adsorbed CO molecules on the surfaces induced by the CO−CO repulsion.

In Figure 4a, the isotherms of the CO coverage (θ_{CO}) on pure Au and Pd surfaces obtained at low temperature (100 K) are reported as a function of $\Delta\mu_{CO}$. In both cases, θ_{CO} increases monotonically with the increase of $\Delta\mu_{CO}$, and three plateaus are observed, which indicates three ordered distributions of CO on the Au and Pd surfaces (see Figure 4b), as is expected for a system with repulsive interactions.[36]

The critical $\Delta\mu_{CO}$ of each ordered phases can be derived from eq 3.6, and we can therefore identify the following stages:

(i) At θ_{CO} = 0.25 ML, the plateau corresponds to an ordered phase in which each CO molecule has two CO molecules in next-nearest-neighbor positions, those that do not share a metal atom. Because $V^{eff}_{CO-CO}(2NB, Metal) = 0$ in this situation, we find

$$\Delta\mu_{CO} = 2V^{eff}_{CO-Metal}$$

(ii) At θ_{CO} = 0.5 ML, the large plateau corresponds to an ordered phase in which each CO molecule finds four CO molecules in next-nearest-neighbor position. Note that for each bridge adsorption site, there are four next-nearest-neighbors but only two of them share a metal atom with it. Once again, because $V^{eff}_{CO-CO}(2NB, Metal) \neq 0$ only if two CO molecules share a metal atom, the maximum number of $V^{eff}_{CO-CO}(2NB, Metal)$ in the present model is two instead of four, and we find

$$\Delta\mu_{CO} = 2V^{eff}_{CO-Metal} + 2V^{eff}_{CO-CO}(2NB, Metal)$$

(iii) At θ_{CO} = 0.75 ML, the plateau corresponds to an ordered phase in which each CO molecule has four CO molecules in next-nearest-neighbor position and two CO molecules in nearest-neighbor position. Therefore

$$\Delta\mu_{CO} = 2V^{eff}_{CO-Metal} + 2V^{eff}_{CO-CO}(2NB, Metal) + 2V^{eff}_{CO-CO}(1NB, Metal)$$

(iv) At θ_{CO} = 1 ML, all the adsorption sites in the adsorbate layer are occupied by CO. The contribution due to V^{eff}_{CO-CO} reaches its maximum value:

$$\Delta\mu_{CO} = 2V^{eff}_{CO-Metal} + 2V^{eff}_{CO-CO}(2NB, Metal) + 4V^{eff}_{CO-CO}(1NB, Metal)$$

Note that the determination of the complete phase diagram of adsorbed CO molecules, (θ_{CO}, T), especially the critical temperatures of the order/disorder phase transitions, goes beyond the scope of this paper.

In Table 4, we report the calculated critical $\Delta\mu_{CO}$, which are in agreement with the MC results: each step increase in θ_{CO} corresponds to one of the calculated critical $\Delta\mu_{CO}$. The existence of CO ordered phases at different θ_{CO} are direct effects of the CO−CO interactions between next-nearest-neighbors, which illustrates the importance of these parameters. Actually, this issue has been often neglected in the theoretical works devoted to the modeling of adsorption-induced segregation.[37,38] Moreover, the repulsion between CO molecules in nearest-neighbor positions is also fixed at arbitrary values. Hence, the effective Hamiltonian derived in the present work allows us to develop a more reliable modeling of the studied system.

Table 4. Values of Critical $\Delta\mu_{CO}$ Obtained from Equation 3.6 Corresponding to the Transitions between the Four Plateaus Found in the Adsorption Isotherms of CO on the Au(100) and Pd(100) Surfaces

θ_{CO} (ML)	0.25	0.50	0.75	1.00
$\Delta\mu_{CO}$ (Au) (eV)	−1.294	−1.074	−0.254	−0.034
$\Delta\mu_{CO}$ (Pd) (eV)	−2.572	−2.072	−0.732	−0.232

3.2.2. CO Adsorption-Induced Segregation in AuPd(100). Surface segregation under different CO partial pressures is studied by performing s-GC Monte Carlo simulations at fixed $\Delta\mu_{CO}$ and variable $\Delta\mu_{AuPd}$ at 300 K. Based on our MC results of CO adsorption on the monometallic surfaces, $\Delta\mu_{CO}$ is chosen to vary from −2.4 to −1.4 eV, which corresponds to CO partial pressures lying in the range of [2×10^{-28} to 2×10^{-11}] torr. Note that according to the value of the alloying pair interaction derived from our DFT calculations, the selected temperature of 300 K is just above the critical temperature of the order/disorder phase transition for the L_{10} structure at c^{bulk}_{Pd} = 0.5 and just below the ones for the L_{12} structures at c^{bulk}_{Pd} = 0.25 and c^{bulk}_{Pd} = 0.75.[39] However, we will see that it has no influence on the results presented in the following.

In Figure 5a we report the isotherms of the surface Pd concentration (c^{surf}_{Pd}), bulk Pd concentration (c^{bulk}_{Pd}), and CO coverage (θ_{CO}) as functions of $\Delta\mu_{AuPd}$. Note that the bulk Pd concentration is obtained from independent bulk calculations to ensure a better precision of this quantity. To help the following discussion, we present also the same coverage and concentration evolutions as functions of c^{bulk}_{Pd} (Figure 5b).

According to the similar trends in the (c^{surf}_{Pd}) and (θ_{CO}) isotherms (Figure 5a,b) one can see that Pd surface segregation is highly affected by $\Delta\mu_{CO}$, with the surface Pd concentration being strongly correlated to the CO coverage. This behavior can be expected from the analysis of the calculated energetic parameters (see section 3.1), which predicted Pd surface segregation induced by CO adsorption. Three main stages can then be defined as a function of $\Delta\mu_{CO}$:

(i) For low CO partial pressure ($\Delta\mu_{CO}$ = −2.4 eV, i.e., P_{CO} = 2×10^{-28} Torr), the surface Pd concentration is always smaller than the bulk Pd concentration, indicating a strong Au surface segregation. This behavior is in agreement with many previous theoretical works about AuPd alloys under vacuum conditions.

(ii) At high CO partial pressure ($\Delta\mu_{CO}$ = −1.4 eV, i.e., P_{CO} = 2×10^{-11} Torr), the segregation isotherm indicates a completely reversed Pd surface segregation, leading to the formation of a pure Pd surface (c^{surf}_{Pd} = 1) upon a pure Au bulk ($c^{bulk}_{Pd} \approx 0$). Moreover, surface saturation by CO gas occurs at intermediate coverage of 0.5 ML, in agreement with many experimental results about CO/Pd(100).[40−42] Actually, using a low-energy electron diffraction technique, Park et al.[40] have shown that CO readily chemisorbs to form a Pd(100) (2 × 4)R45 CO structure at room temperature, with one CO molecule adsorbed to every two surface Pd atoms in an alternating bridged bond arrangement.

(iii) At intermediate CO partial pressures ($\Delta\mu_{CO}$ = −1.8 eV, i.e., $P_{CO} = 3 \times 10^{-18}$ Torr), original isotherms are found. Within this pressure range, the surface Pd concentration and the CO coverage both slowly increase with increasing c^{bulk}_{Pd} and a reversed Pd segregation is still observed ($c^{surf}_{Pd} > c^{bulk}_{Pd}$) on the whole range of c^{bulk}_{Pd}. In addition, a plateau is found before c^{surf}_{Pd} reaches 1, indicating the existence of an ordered phase. Note that this surface ordered phase cannot be due to an ordering in the bulk due to the chosen low temperature of 300 K relative to

DOI: 10.1021/acs.jpcc.5b10158
J. Phys. Chem. C 2016, 120, 350−359

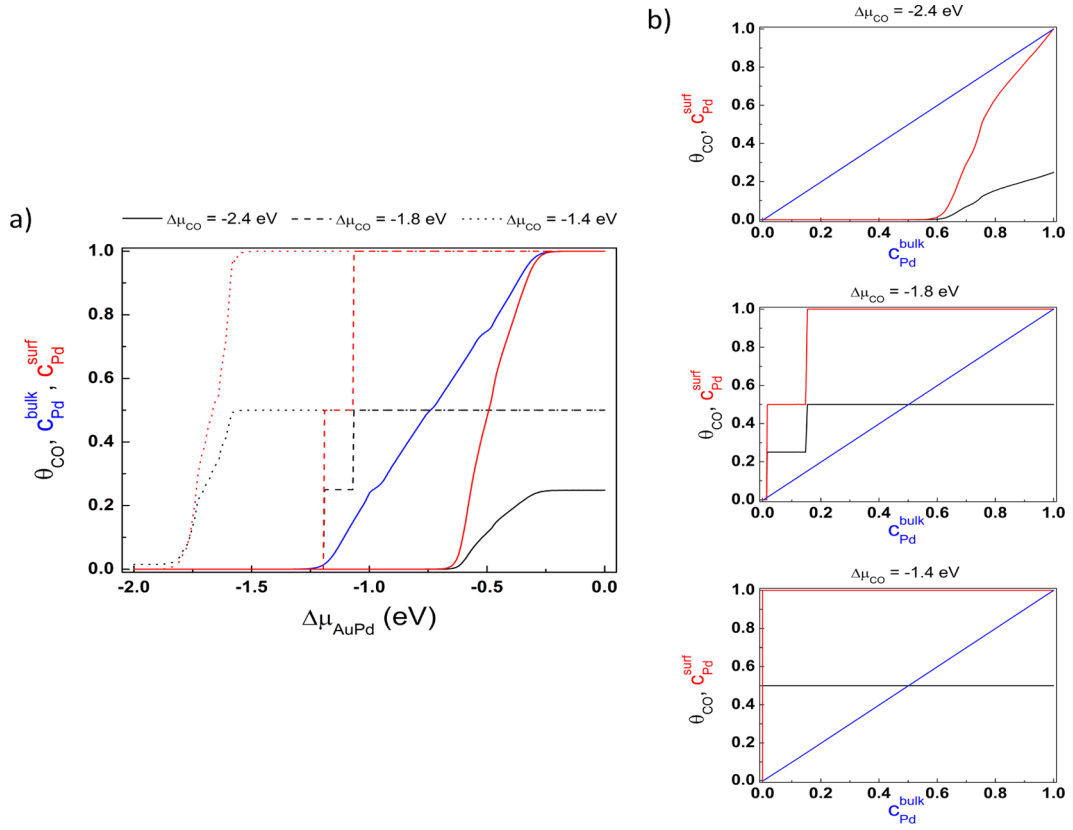

Figure 5. (a) Isotherms at T = 300 K representing the evolutions of the CO coverage (θ_{CO}, black), surface Pd concentration (c_{Pd}^{surf}, red), and bulk Pd concentration (c_{Pd}^{bulk}, blue) as functions of $\Delta\mu_{AuPd}$ at three given $\Delta\mu_{CO}$ (−2.4, −1.8, and −1.4 eV). (b) Evolutions of the CO coverage (θ_{CO}, black) and surface Pd concentration (c_{Pd}^{surf}, red) as functions of c_{Pd}^{bulk} at three given $\Delta\mu_{CO}$ (−2.4, −1.8, and −1.4 eV) at T = 300 K. The first diagonal corresponds to the bulk Pd concentration.

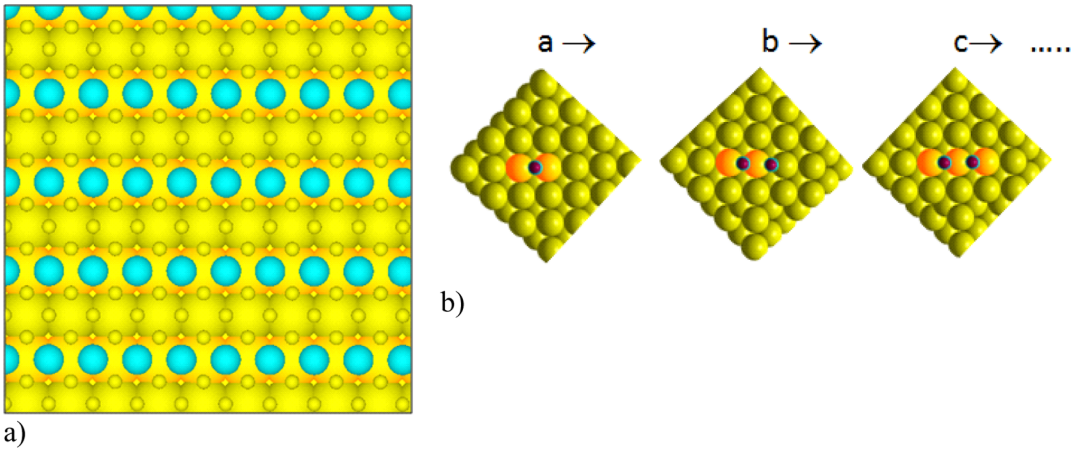

Figure 6. (a) Ordered configuration corresponding to the plateau observed in the isotherm of the surface Pd concentration at $\Delta\mu_{CO}$ = −1.8 eV. (b) Sketch map of the formation of Pd linear chains in the Au(100) surface.

the critical temperatures of order/disorder transitions because the plateau in c_{Pd}^{surf} lies between c_{Pd}^{bulk} = 0.01 and c_{Pd}^{bulk} = 0.16 where bulk AuPd is in a disordered state.[39] The corresponding ordered configuration, reported in Figure 6 a, shows Pd atoms forming linear chains in the surface with adsorbed CO molecules, separated by Au atoms forming also linear chains free of adsorbed CO molecules. The corresponding surface Pd concentration and the CO coverage are 0.5 and 0.25 ML, respectively.

The exotic ordered phase at θ_{CO} = 0.25 ML is due both to the ordering of CO adsorbed molecules on the surface of the alloy (CO−CO repulsion) and to the different CO−metal interactions between Au and Pd. Figure 6b shows a sketch map to understand the formation mechanism of the Pd chains on the alloy surface. The question is once a CO molecule is adsorbed on a Pd−Pd bridge site, where will a second CO molecule adsorb preferentially? A first possibility could be an adsorption over an isolated Au−Au bridge site, which involves 2 CO−Au interactions and no CO−CO repulsive interaction. A

DOI: 10.1021/acs.jpcc.5b10158
J. Phys. Chem. C 2016, 120, 350−359

second possibility could be an adsorption at a neighboring Au−Pd bridge site, which involves one CO−Au interaction, one CO−Pd interaction, and one CO−CO repulsive interaction. Therefore, the competition is between the CO−metal interactions ($\Delta V^{\mathrm{eff}}_{\mathrm{CO-metal}} = V^{\mathrm{eff}}_{\mathrm{CO-Pd}} - V^{\mathrm{eff}}_{\mathrm{CO-Au}}$) and an additional CO−CO repulsion. According to our DFT results, $\Delta V^{\mathrm{eff}}_{\mathrm{CO-metal}}$ is 0.64 eV and the maximum CO−CO repulsion is 0.46 eV. Hence, the CO−metal interaction primes and the second CO molecule will bind preferentially to a Pd atom which is shared with another CO molecule instead of adsorbing on a vacant Au bridge site. Furthermore, the system tries to minimize the contribution of the CO−CO repulsive interactions by being located at a next-nearest-neighbor position, as shown in Figure 6b. This is the key point to form a one-dimensional chain instead of two-dimensional islands on the surface. Consequently, the new adsorbed CO molecule will not be satisfied by being adsorbed on an Au−Pd bridge site and will draw another Pd atom in the surface plane to form a Pd−Pd bridge site. Thus, it triggers a domino effect and results in the formation of Pd linear chains, behavior that needs the detailed description of the CO−CO interactions developed in this work.

The prediction and the control of this ordered AuPd structure is highly interesting for catalysis design and it could offer original active sites for many catalytic reactions. Moreover, the predicted Pd chains could be related to the observed increasing rate of the CO oxidation reaction on AuPd(100) in the work of Goodman and co-workers.[17] More precisely, using IR spectroscopy, these authors show an increase of the number of surface contiguous Pd atoms with CO adsorbed on the Pd−Pd bridge site when the CO pressure is higher than about 0.1 Torr. They observe an increase of the band located around 1990 cm^{-1}, which they tentatively assign to Pd−Pd bridging CO with other CO molecules in neighboring bridging sites, when the CO pressure increases. In addition to this observation, the authors record an increase of the CO oxidation rate when contiguous Pd atoms are formed on the surface. They explain that the contiguous Pd atoms are responsible for the dissociation of the O_2 molecules and by consequence for the enhanced activity of the CO oxidation reaction. Our results evidencing the promising AuPd surface ordering are in line with the experimental IR observations. In addition, in line with Goodman's prediction, this surface configuration presenting Pd linear chains could help the dissociation of O_2 at low temperature, while the Au chains in between offer weak CO adsorption sites which can react to form CO_2.

4. CONCLUSIONS

In this work, we develop a theoretical method that is able to treat accurately both segregation and adsorption for alloyed metallic systems exposed to gas. For the present case of Au−Pd(100) surface with adsorbed CO molecules, DFT calculations are performed to define energetic quantities that describe metal−metal, metal−CO, and CO−CO interactions. Based on an Ising model, a relationship between CO adsorption and the local Pd surface concentration is established. The results show a determinant effect of the CO−CO interactions and reveal a competition between the CO−metal interactions and the CO−CO repulsions. Hence, in addition to the evidence of a reversed Pd segregation induced by CO adsorption, we find the existence of an interesting ordered phase. Indeed, for surface Pd concentration close to 0.5 and CO coverage of about 0.25 ML, an ordered configuration appears at room temperature in which Pd atoms form parallel linear chains with adsorbed CO molecules separated by CO-free Au parallel linear chains. This ordered phase is highly interesting for catalysis design and it could offer original active sites for many catalytic reactions.

AUTHOR INFORMATION

Corresponding Authors

*E-mail: hazar.guesmi@enscm.fr.

*E-mail: zhubeien@sinap.ac.cn.

Notes

The authors declare no competing financial interest.

ACKNOWLEDGMENTS

The authors acknowledge the financial support from the French Agence Nationale de la Recherche (ANR) under reference ANR-11-JS07-0007 and EU (COST-MP0903). This work was granted access to the HPC resources of [CCRT/CINES/IDRIS] under the allocation 2014 [x2014086395] made by GENCI (Grand Equipement National de Calcul Intensif]. B.Z. also acknowledges the Development Fund for Shanghai Talents.

REFERENCES

(1) Woodruff, D. P. *The Chemical Physics of Solid Surfaces. Alloy Surfaces and Surface Alloys*; Elsevier: Amsterdam, 2002.

(2) Delannoy, L.; Thrimurthulu, G.; Reddy, P. S.; Méthivier, C.; Nelayah, J.; Reddy, B. M.; Ricolleau, C.; Louis, C. Selective Hydrogenation of Butadiene over TiO2 Supported Copper, Gold and Gold−Copper Catalysts Prepared by Deposition−Precipitation. *Phys. Chem. Chem. Phys.* **2014**, *16*, 26514−26527.

(3) Morfin, F.; Nassreddine, S.; Rousset, J. L.; Piccolo, L. Nanoalloying Effect in the Preferential Oxidation of CO over Ir−Pd Catalysts. *ACS Catal.* **2012**, *2*, 2161−2168.

(4) Vestergaard, E. K.; Vang, R. T.; Knudsen, J.; Pedersen, T. M.; An, T.; Laegsgaard, E.; Stensgaard, I.; Hammer, B.; Besenbacher, F. Adsorbate-Induced Alloy Phase Separation: a Direct View by High-Pressure Scanning Tunneling Microscopy. *Phys. Rev. Lett.* **2005**, *95*, 126101.

(5) Tao, F.; Grass, M. E.; Zhang, Y.; Butcher, D. R.; Renzas, J. R.; Liu, Z.; Chung, J. Y.; Mun, B. S.; Salmeron, M.; Somorjai, G. A. Reaction-Driven Restructuring of Rh-Pd and Pt-Pd Core-Shell Nanoparticles. *Science* **2008**, *322*, 932−934.

(6) Xin, H. L.; Alayoglu, S.; Tao, S.; Genc, A.; Wang, C.-M.; Kovarik, L.; Stach, E. A.; Wang, L.-W.; Salmeron, M.; Somorjai, G. A.; Zheng, H. Revealing the Atomic Restructuring of Pt−Co Nanoparticles. *Nano Lett.* **2014**, *14*, 3203−3207.

(7) Ferrando, R. Symmetry Breaking and Morphological Instabilities in Core-Shell Metallic Nanoparticles. *J. Phys.: Condens. Matter* **2015**, *27*, 013003−013038.

(8) Ferrando, R.; Jellinek, J.; Johnston, R. L. Nanoalloys: From Theory to Applications of Alloy Clusters and Nanoparticles. *Chem. Rev.* **2008**, *108*, 845−910.

(9) Zhu, B.; Guesmi, H.; Creuze, J.; Legrand, B.; Mottet, C. Crossover Among Structural Motifs in Pd−Au Nanoalloys. *Phys. Chem. Chem. Phys.* **2015**, *17*, 28129−28136.

(10) Guesmi, H. Theoretical Insights on the Effect of Reactive Gas on the Chemical Ordering of Gold-Based Alloys. *Gold Bull.* **2013**, *46*, 213−220.

(11) Schmick, H. D.; Wassmuth, H. W. Adsorption, Desorption and Reaction Kinetics of Nitric Oxide on a Stepped Pd(111) Surface. *Surf. Sci.* **1982**, *123*, 471−490.

(12) Chau, T. D.; Visart de Bocarmé, T.; Kruse, N. Formation of N_2O and $(NO)_2$ During NO Adsorption on Au 3D Crystals. *Catal. Lett.* **2004**, *98*, 85−87.

(13) Engel, T.; Ertl, G. Elementary Steps in the Catalytic Oxidation of Carbon Monoxide on Platinum Metals. *Adv. Catal.* **1979**, *28*, 1−73.

DOI: 10.1021/acs.jpcc.5b10158
J. Phys. Chem. C 2016, 120, 350−359

(14) Rousset, J. L.; Bertolini, J. C.; Miegge, P. Theory of Segregation Using the Equivalent-Medium Approximation and Bond-Strength Modifications at Surfaces: Application to FCC Pd-X Alloys. *Phys. Rev. B: Condens. Matter Mater. Phys.* **1996**, *53*, 4947−4957.
(15) Liu, H. B.; Pal, U.; Medina, A.; Maldonado, C.; Ascencio, J. A. Structural Incoherency and Structure Reversal in Bimetallic Au-Pd Nanoclusters. *Phys. Rev. B: Condens. Matter Mater. Phys.* **2005**, *71*, 075403.
(16) Gao, F.; Wang, Y.; Goodman, D. W. CO Oxidation over AuPd(100) from Ultrahigh Vacuum to Near-Atmospheric Pressures: CO Adsorption-Induced Surface Segregation and Reaction Kinetics. *J. Phys. Chem. C* **2009**, *113*, 14993−15000.
(17) Gao, F.; Wang, Y.; Goodman, D. W. CO Oxidation over AuPd(100) from Ultrahigh Vacuum to Near-Atmospheric Pressures: The Critical Role of Contiguous Pd Atoms. *J. Am. Chem. Soc.* **2009**, *131*, 5734−5735.
(18) Zhu, B.; Thrimurthulu, T.; Delannoy, L.; Louis, C.; Mottet, C.; Creuze, J.; Legrand, B.; Guesmi, H. Evidence of Pd Segregation and Stabilization at Edges of AuPd Nano-clusters in the Presence of CO: a Combined DFT and DRIFTS Study. *J. Catal.* **2013**, *308*, 272−281.
(19) Sansa, M.; Dhouib, A.; Guesmi, H. Density Functional Theory Study of CO-Inducing Segregation in Gold-Based Alloys. *J. Chem. Phys.* **2014**, *141*, 064709−064717.
(20) Guesmi, H.; Louis, C.; Delannoy, L. Chemisorbed Atomic Oxygen Inducing Pd Segregation in PdAu Alloy: Energetic and Electronic DFT Analysis. *Chem. Phys. Lett.* **2011**, *503*, 97−100.
(21) Dhouib, A.; Guesmi, H. DFT Study of the M Segregation on MAu Alloys (M = Ni, Pd, Pt) in Presence of Adsorbed Oxygen O and O_2. *Chem. Phys. Lett.* **2012**, *521*, 98−103.
(22) Creuze, J.; Guesmi, H.; Mottet, C.; Zhu, B.; Legrand, B. Superficial Segregation in AuPd Alloys: Ab initio Analysis of the Driving Forces. *Surf. Sci.* **2015**, *639*, 48−53.
(23) Berthier, F.; Legrand, B.; Tréglia, G. How to Compare Superficial and Intergranular Segregation? A New Analysis within the Mixed SMA−TBIM Approach. *Acta Mater.* **1999**, *47*, 2705−2715.
(24) Creuze, J.; Braems, I.; Berthier, F.; Mottet, C.; Tréglia, G.; Legrand, B. Model of Surface Segregation Driving Forces and their Coupling. *Phys. Rev. B: Condens. Matter Mater. Phys.* **2008**, *78*, 075413.
(25) Kresse, G.; Hafner, J. Ab initio Molecular Dynamics for Liquid Metal. *Phys. Rev. B: Condens. Matter Mater. Phys.* **1993**, *47*, 558−561.
(26) Perdew, J. P.; Zunger, A. Self-Interaction Correction to Tensity-Functional Approximations for Many-Electron Systems. *Phys. Rev. B: Condens. Matter Mater. Phys.* **1981**, *23*, 5048−5079.
(27) Blochl, P. E.; Jepsen, O.; Andersen, O. K. Improved Tetrahedron Method for Brillouin-Zone Integrations. *Phys. Rev. B: Condens. Matter Mater. Phys.* **1994**, *49*, 16223−16234.
(28) Kresse, G.; Joubert, D. From Ultrasoft Pseudopotentials to the Projector Augmented-Wave Method. *Phys. Rev. B: Condens. Matter Mater. Phys.* **1999**, *59*, 1758−1775.
(29) Frenkel, D.; Smit, B. *Understanding Molecular Simulation*; Academic Press: New York, 1995.
(30) *JANAF Thermodynamical Tables*; Stull, D. R., Prophet, H.; National Bureau of Standards: Washington, DC, 1971.
(31) Metropolis, N.; Rosenbluth, A. W.; Rosenbluth, M. N.; Teller, A. H.; Teller, E. Equation of State Calculations by Fast Computing Machines. *J. Chem. Phys.* **1953**, *21*, 1087−1092.
(32) Kittel, Ch. *Introduction to Solid State Physics*, 7th ed.; Wiley: New York, 1996.
(33) Skriver, H. L.; Rosengaard, N. M. Surface Energy and Work Function of Elemental Metals. *Phys. Rev. B: Condens. Matter Mater. Phys.* **1992**, *46*, 7157−7168.
(34) Montemore, M. M.; Medlin, J. W. A Unified Picture of Adsorption on Transition Metals Through Different Atoms. *J. Am. Chem. Soc.* **2014**, *136*, 9272−9284.
(35) Calle-Vallejo, F.; Loffreda, D.; Koper, M. T. M.; Sautet, P. Introducing Structural Sensitivity into Adsorption−Energy Scaling Relations by Means of Coordination Numbers. *Nat. Chem.* **2015**, *7*, 403−410.
(36) Patrykiejew, A.; Sokołowski, S.; Binder, K. Phase Transitions in Adsorbed Layers Formed on Crystals of Square and Rectangular Surface Lattice. *Surf. Sci. Rep.* **2000**, *37*, 207−344.
(37) Christoffersen, E.; Stoltze, P.; Nørskov, J. K. Monte Carlo Simulations of Adsorption-Induced Segregation. *Surf. Sci.* **2002**, *505*, 200−214.
(38) Han, B. C.; Van der Ven, A.; Ceder, G.; Hwang, B.-J. Surface Segregation and Ordering of Alloy surfaces in the Presence of Adsorbates. *Phys. Rev. B: Condens. Matter Mater. Phys.* **2005**, *72*, 205409.
(39) Binder, K. Ordering of the Face-Centered-Cubic Lattice with Nearest-Neighbor Interaction. *Phys. Rev. Lett.* **1980**, *45*, 811.
(40) Park, R.; Madden, H. H., Jr. Annealing Changes on the (100) Surface of Palladium and their Effect on CO Adsorption. *Surf. Sci.* **1968**, *11*, 188−202.
(41) Tracy, J. C.; Palmberg, P. W. Structural Influences on Adsorbate Binding Energy. Part-1: Carbon Monoxide on (100) Palladium. *J. Chem. Phys.* **1969**, *51*, 4852−4862.
(42) Ortega, A.; Huffman, F. M.; Bradshaw, A. M. The Adsorption of CO on Pd(100) Studies by IR Reflection Adsorption Spectroscopy. *Surf. Sci.* **1982**, *119*, 79−94.

DOI: 10.1021/acs.jpcc.5b10158
J. Phys. Chem. C 2016, 120, 350−359